

Solid-State Reaction Kinetics of the System CaO-FeO

HIROYUKI FUKUYAMA, Md. KHALID HOSSAIN, and KAZUHIRO NAGATA

The solid-state reaction mechanisms of the CaO-FeO system have been studied by a diffusion couple method in the temperature range of 1073 to 1273 K, under controlled oxygen-partial pressures. The interdiffusivities and intrinsic diffusivities of Ca^{2+} and Fe^{2+} have been determined in the limited FeO solid-solution range. Based on the obtained results, a solid-state reaction model of the system has been developed, taking account of the formation of the $\text{Ca}_2\text{Fe}_2\text{O}_5$ phase. According to the model, the diffusivities of Fe^{3+} in the $\text{Ca}_2\text{Fe}_2\text{O}_5$ phase have been estimated at 1273 K.

I. INTRODUCTION

THE free lime (free CaO) remaining in the refining slag in the steel industry makes an adverse effect on its recycling due to the hydration of lime.^[1,2] There are some investigations on the effect of FeO dissolved in free CaO on the hydration. Matsunaga *et al.*^[1] reported that in rapidly cooled slag, FeO segregates on the surface of the free-CaO phase and acts as a coating against hydration. Allen and Snow^[3] also have reported that free CaO became more resistant to atmospheric hydration by the dissolution of FeO. In case of slowly cooled slag, the FeO seems to be homogeneously distributed in the free-CaO phase, and the hydration of the free CaO becomes easier. Thus, the solid-state reaction kinetics between CaO and FeO is important from the viewpoint of effective slag recycling.

A large number of investigations of the CaO-iron oxide system have been reported in the literature.^[4–16] Some reports were published relating to the solid-state diffusion kinetics of the CaO- Fe_2O_3 system^[12,13], and self-diffusion^[14,15] and impurity diffusion^[16] relating to crystalline CaO and FeO. However, there are no data in the literature for the interdiffusivity of the CaO-FeO system.

Thus, in the present article, the CaO-FeO system is studied with the aim of evaluating the kinetic behavior in the solid state by the diffusion couples composed of single crystalline CaO and unidirectional crystalline FeO.

II. EXPERIMENTAL

A. CaO-FeO System

There has been controversy regarding the CaO-FeO phase diagram. In 1955, Allen and Snow^[3] presented the phase diagram of the CaO-FeO system in equilibrium with metallic iron. According to their study, the system consists of CaO and FeO solid solutions with limited mutual-solid solubility and dicalcium ferrite ($\text{Ca}_2\text{Fe}_2\text{O}_5$), and the system is not eutectic. The lowest liquidus point is 1381 K at a composition of 26 mass pct CaO-74 mass pct FeO, which is the maximum solubility of CaO in FeO, and the dicalcium ferrite incongruently melts approximately at 1353 K. Abbatista *et al.*^[5] in

1975 presented results supporting the phase diagram reported by Allen and Snow, although the decomposition temperature of dicalcium ferrite is lower by 30 K than that reported by them.

On the other hand, Schürmann and Kraume^[7] in 1976 concluded that the CaO-FeO section with metallic iron saturation presents the eutectic type characterized by the ternary eutectic equilibrium of Fe-CaO solid solution- $\text{Ca}_2\text{Fe}_2\text{O}_5$. The solubility limit of CaO in FeO is approximately 12 mass pct, and the $\text{Ca}_2\text{Fe}_2\text{O}_5$ incongruently melts at 1423 K.

In 1988, Bergman and Song^[8] studied the Ca-Fe-O system and concluded that the system is not eutectic, supporting the phase diagram suggested by Abbatista *et al.*^[5] On this major disagreement, Bergman and Song pointed out that the eutecticlike structure interpreted by Schürmann and Kraume^[7] was actually results of the eutectoid-decomposition of wüstite occurring during cooling.

In the present study, solid-state reaction kinetics of the CaO-FeO system was studied by a diffusion couple method at temperatures ranging from 1073 to 1273 K, which is below the decomposition temperature of $\text{Ca}_2\text{Fe}_2\text{O}_5$ based on the preceding investigations,^[3,5,7,8] although some disagreements are among the phase diagrams. Oxygen partial pressures were carefully determined so as to be slightly higher than that of Fe/FeO equilibrium at respective temperatures based on the FeO- Fe_2O_3 phase diagram reported by Phillips and Muan^[17] as presented in Table I.

B. Sample Preparation

FeO was prepared by the oxidation of an iron plate ($0.50 \times 15 \times 100$ mm, 99.99 mass pct) under controlled oxygen-partial pressure of 10^{-8} Pa at 1373 K for 86.4 ks by CO/ CO_2 gas mixtures. The product was confirmed as a single phase of FeO by X-ray diffractometry. The FeO crystals on the iron plate were unidirectionally developed. Figure 1 shows the optical micrograph of the FeO crystals. A diffusion sample of FeO was cleaved from the plate of FeO crystals. The size of the FeO sample was about $4 \times 4 \times 0.25$ mm having approximately 2 to 4 crystal grains.

CaO single crystal with (111) plane orientation was used for the diffusion experiment. A small piece of CaO was cut by cleavage similar in size as the FeO sample. The samples of FeO and CaO were polished with number 4000 SiC polishing papers and Al_2O_3 powder of $0.3 \mu\text{m}$ and finished with ultrasonic cleaning in acetone.

HIROYUKI FUKUYAMA, Associate Professor, Md. KHALID HOSSAIN, former Graduate Student, and KAZUHIRO NAGATA, Professor, are with the Department of Chemistry and Materials Science, Tokyo Institute of Technology, Tokyo 152-8552, Japan. Contact e-mail: fukuyama@mtl.titech.ac.jp

Manuscript submitted August 8, 2001.

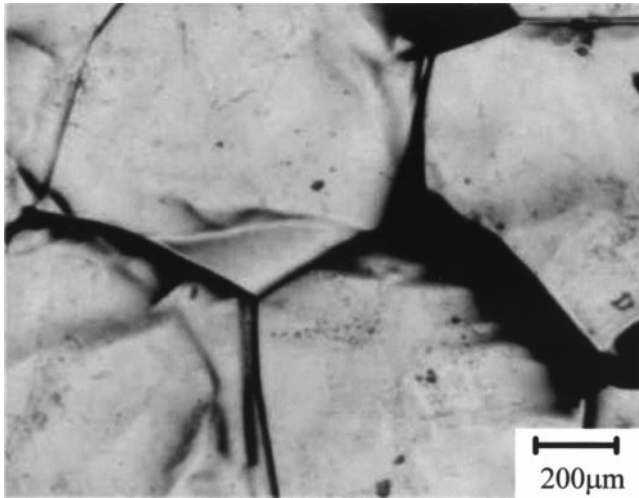


Fig. 1—Optical micrograph of the surface of FeO crystals prepared by the oxidation of iron plate with $P_{O_2} = 10^{-8}$ Pa at 1373 K for 86.4 ks.

Table I. Condition for Diffusion Experiment

| Run | Temperature (K) | Time (ks) | p_{O_2} (Pa) |
|-----|-----------------|-----------|---------------------|
| 1* | 1273 | 0.3 | 1×10^{-10} |
| 2* | 1273 | 0.6 | 1×10^{-10} |
| 3 | 1273 | 1.2 | 1×10^{-10} |
| 4 | 1273 | 1.8 | 1×10^{-10} |
| 5* | 1273 | 3.6 | 1×10^{-10} |
| 6* | 1273 | 7.2 | 1×10^{-10} |
| 12* | 1173 | 1.2 | 2×10^{-12} |
| 13 | 1173 | 1.8 | 2×10^{-12} |
| 14* | 1173 | 2.4 | 2×10^{-12} |
| 15* | 1173 | 3.6 | 2×10^{-12} |
| 16 | 1073 | 1.8 | 1×10^{-14} |

*Platinum marker experiment.

C. Diffusion Experiment

The polished FeO and CaO samples were placed face-to-face to make a diffusion couple. Proper contact was assured by placing the diffusion couple into a spring-loaded, push-rod sample holder. After attaining the experimental temperature, the diffusion sample was put in the upper cool part of a reaction tube in a furnace. Then, the CO/CO₂ gas mixture was introduced in the reaction tube. After attaining the desired oxygen-partial pressure, the diffusion couple was pushed to the highest temperature region of the furnace, which permitted the interdiffusion. The diffusion experiments were performed with the conditions presented in Table I. After the diffusion annealing, the sample was quenched by pushing it to the cooled-end of the furnace.

The diffused samples were cut perpendicular to the original interface with a diamond-tipped fine saw. The sectioned surface was polished with number 4000 SiC polishing papers and 0.3- μm Al₂O₃ powder. The polished diffusion interface was observed by an optical microscope. The quantitative analysis was performed across the diffusion couple perpendicular to the diffusion interface by electron probe microanalysis (EPMA). An electron volt of 20 kV and specimen current of 30 nA was used for the analysis. The beam size used is 1 μm . The intensities of the characteristics X-rays

(Fe K_{α} and Ca K_{α}) were measured with 1 to 5 μm intervals near the diffusion interface and with 10 to 50 μm intervals far from the interface. Diffusion experiments were also conducted using the sample coated with platinum paste at the interface of the diffusion couple as the Kirkendall marker to determine the intrinsic diffusivities.

D. Boltzmann–Matano Analysis for Multiphase System

The concentration vs distance profiles for the CaO–FeO diffusion couples were analyzed by the Boltzmann–Matano method^[18] to determine the variation of interdiffusivity with concentration. Fick's second law of diffusion in the one-dimensional case can be written as

$$\frac{\partial c}{\partial t} = \frac{\partial}{\partial x} \left(D \frac{\partial c}{\partial x} \right) \quad [1]$$

where c is concentration in mol/m³ as a function of distance, x , and time, t ; and D is the interdiffusivity. Initial conditions are

$$c = c_0 \text{ for } x < 0, \text{ at } t = 0 \quad [2]$$

$$c = 0 \text{ for } x > 0, \text{ at } t = 0 \quad [3]$$

In the FeO–CaO system, the diffusion profiles show discontinuity, as illustrated in Figure 2, because of the appearance of the Ca₂Fe₂O₅ phase. The solution of the diffusion equation then is obtained by solving a three-phase-two-moving-boundary problem. A modification of the Boltzmann–Matano solution was carried out by Jost^[19] and Appel^[20] to provide the mathematical solution to determine the Matano interface. As applied to Figure 2, this can be expressed as

$$\int_0^{c_1} xdc + (c_2 - c_1)x_{1,2} + \int_{c_2}^{c_3} xdc \quad [4]$$

$$+ (c_4 - c_3)x_{2,3} + \int_{c_4}^{c'} xdc = 0$$

With the Matano interface, the interdiffusivity, $D(c')$, at a given concentration, c' , can be obtained from the graphical integration and differentiation of $c(x)$ using the equation

$$D(c') = -\frac{1}{2t} \left(\frac{dx}{dc} \right)_{c'} \left[\int_0^{c_1} xdc + (c_2 - c_1)x_{1,2} \quad [5]$$

$$+ \int_{c_2}^{c_3} xdc + (c_4 - c_3)x_{2,3} + \int_{c_4}^{c'} xdc \right]$$

Jost^[19] has shown that the application of the Boltzmann–Matano analysis to multiphase diffusion is valid for diffusing systems in which a finite number of discontinuities occur in the concentration and in the diffusion coefficient. Appel^[20] has emphasized that the preceding solutions are only valid if the process involved is diffusion, so that concentration is only a function of $x/t^{1/2}$.

E. Intrinsic Diffusivity

The interdiffusivity, D , is related to the intrinsic diffusivities, $D_{Ca^{2+}}$ and $D_{Fe^{2+}}$ by Darken's Equation:^[21]

$$D = (N_{FeO}D_{Ca^{2+}} + N_{CaO}D_{Fe^{2+}}) \quad [6]$$

where N_{FeO} and N_{CaO} are the molar fractions of FeO and CaO,

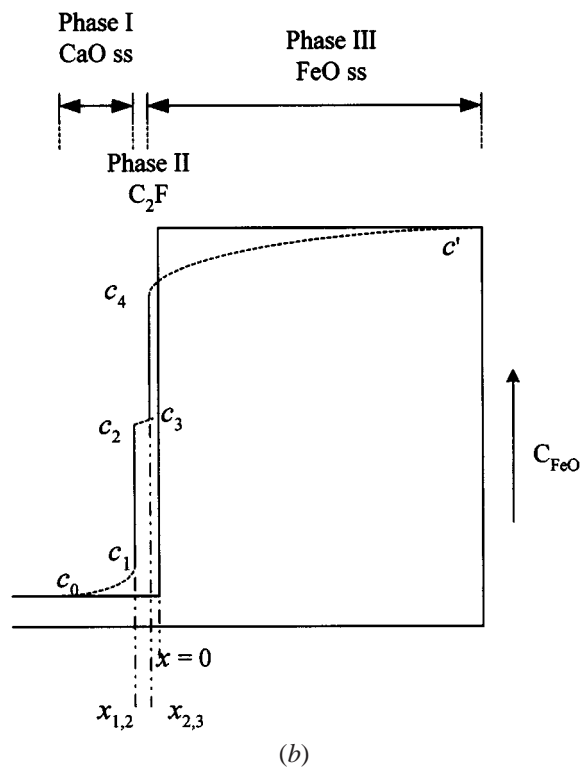
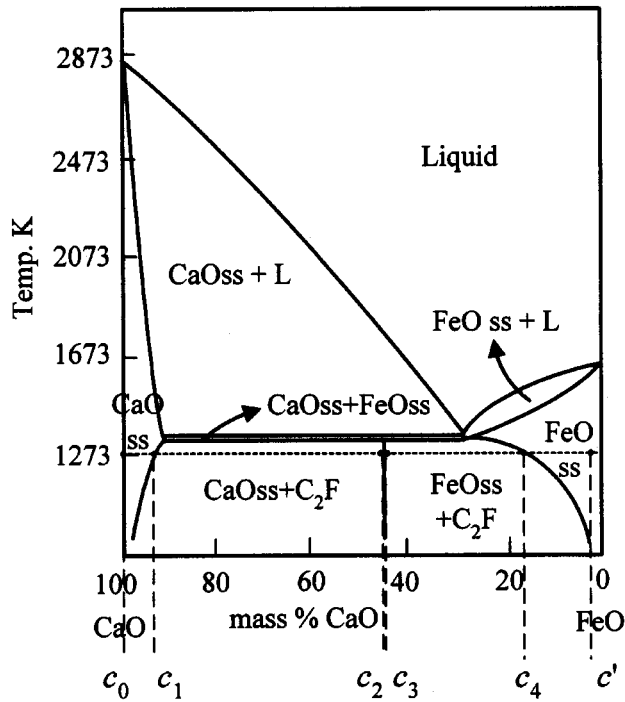


Fig. 2—(a) CaO-FeO phase diagram^[3,6] and (b) schematic diffusion profile for three-phase diffusion problem. $C_2F = Ca_2Fe_2O_5$.

respectively. These intrinsic diffusivities are also related to the marker velocity, v , as follows:

$$v = (D_{Fe^{2+}} - D_{Ca^{2+}}) \frac{\partial N_{FeO}}{\partial x} \quad [7]$$

Therefore, the intrinsic diffusivities are calculated from the interdiffusivity and the marker velocity by the combination of Eqs. [6] and [7]. The marker velocity can be obtained by the manner described by Darken.^[21] The shift of the marker, x_m , is given by the expression

$$x_m = It^{1/2} \quad [8]$$

where I is a function of $x/t^{1/2}$. Thus, the velocity is given by the following equation:

$$v = \frac{dx_m}{dt} = \frac{1}{2} It^{-1/2} = \frac{x_m}{2t} \quad [9]$$

The marker velocity is calculated from x_m , which is the distance between the marker interface and the Matano interface.

III. RESULTS

A. Growth of Intercompound, $Ca_2Fe_2O_5$

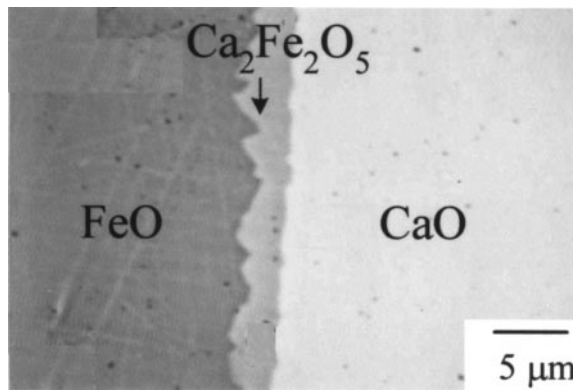
The cross-sectional views of the diffusion interface annealed with $P_{O_2} = 10^{-10}$ Pa at 1273 K for 1.8 ks are shown in Figure 3. $Ca_2Fe_2O_5$ phase as an intercompound can be found at the interface. The $Ca_2Fe_2O_5$ phase always existed at the interface during the course of diffusion in all diffusion experiments. It should be noted that the interface between the $Ca_2Fe_2O_5$ and the FeO shows a zigzag shape compared with the other side. Due to the zigzag shape of the $Ca_2Fe_2O_5$ layer, the average thickness of the layer was calculated from the area of the layer, which was estimated graphically. The thickness against the square root of diffusion time represents a linear relation, as shown in Figure 4, which indicates the growth process as diffusion controlled. The zigzag shape of the $Ca_2Fe_2O_5$ formed is due to the dissolution of $Ca_2Fe_2O_5$ in the FeO solid solution, which is explained in Section IV.

B. Marker Movement

Figure 5 shows the cross-sectional view of diffusion interface after the marker experiments at 1273 K for 3.6 ks. Pt marker particles can be found in the FeO phase. The diffusion profile with marker position is represented in Figure 6 for the sample annealed at 1273 K for 0.6 ks. As can be seen in Figure 6, the diffusion profile shows a limited mutual-solid solubility between FeO and CaO. In the FeO solid-solution layer, a long tailing of concentration was observed compared with that in the CaO solid-solution layer. The shift of marker with reference to the Matano interface was calculated. The marker shift against the square root of the diffusion time presents a linear relation, as shown in Figure 7, which indicates that the position of the marker is a function of $x/t^{1/2}$, that is, it is diffusion-controlled.

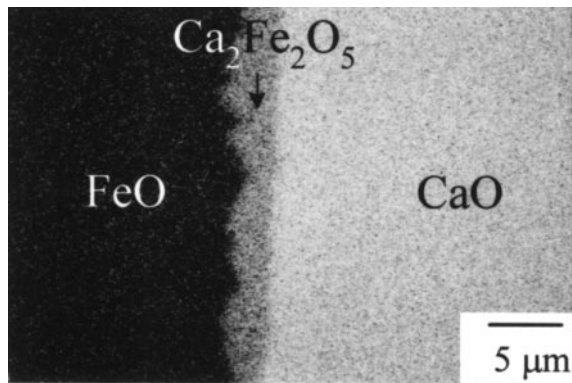
C. Penetration Curve

Profiles of molar fraction of CaO against distance normalized with $t^{1/2}$ are shown in Figure 8 for the samples for $t = 0.3, 0.6, 1.2,$ and 1.8 ks at 1273 K. If local equilibrium was established throughout, the profiles should be identical.



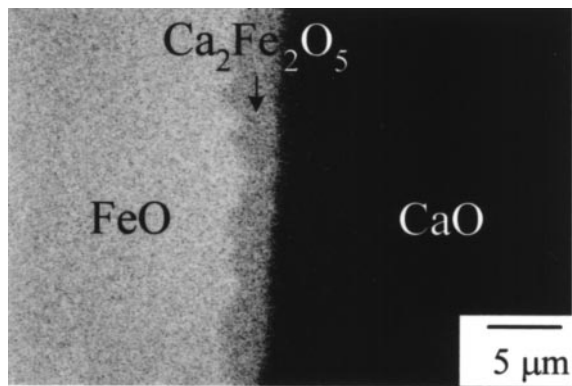
SC image

(a)



Ca mapping

(b)



Fe mapping

(c)

Fig. 3—EPMA micrographs showing a cross-sectional view of the diffusion interface annealed with $P_{O_2} = 10^{-10}$ Pa at 1273 K for 1.8 ks.

Thus, the relationships shown in the figure uphold the validity of the use of Boltzmann–Matano analysis for the present system. The same conclusion was obtained for the experiments conducted at other temperatures.

In the present study, the solubilities of CaO in the FeO

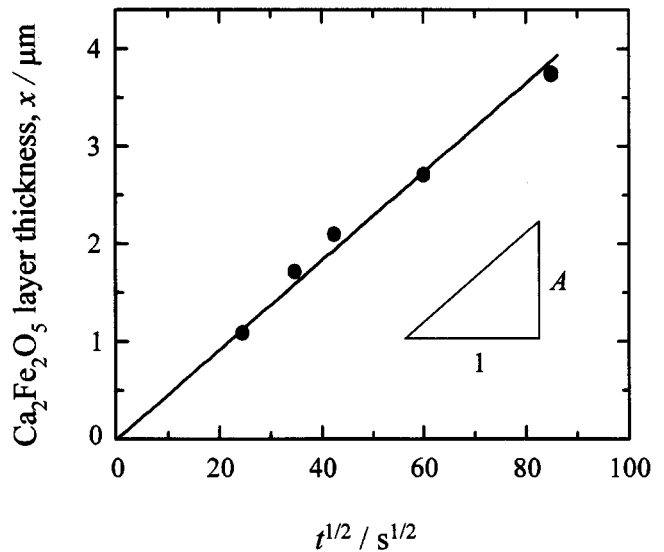


Fig. 4—Thickness of $Ca_2Fe_2O_5$ layer as a function of the square root of diffusion time at 1273 K with $P_{O_2} = 10^{-10}$ Pa.

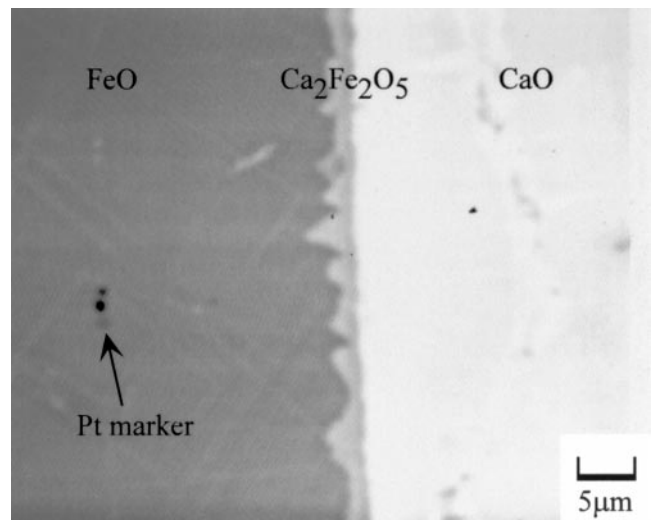


Fig. 5—Cross-sectional view of the diffusion interface with Pt marker for the sample annealed with $P_{O_2} = 10^{-10}$ Pa at 1273 K for 3.6 ks.

phase are approximately 0.15 and 0.10 in molar fraction of CaO at 1273 and 1173 K, respectively, which are close to those reported by Allen and Snow.^[3]

D. Interdiffusivity

The concentration dependencies of the interdiffusivities are shown in Figure 9. The interdiffusivities have been determined up to the CaO solubility in FeO phase because the penetration profile in CaO phase was very narrow. The values of $\log D$ for different concentrations are plotted against the reciprocal temperature in Figure 10. The temperature dependence of the diffusivity demonstrates the Arrhenius-type equation:

$$D = D_0 \exp(-Q/RT) \quad [10]$$

where Q is the apparent activation energy in J/mol, D_0 is

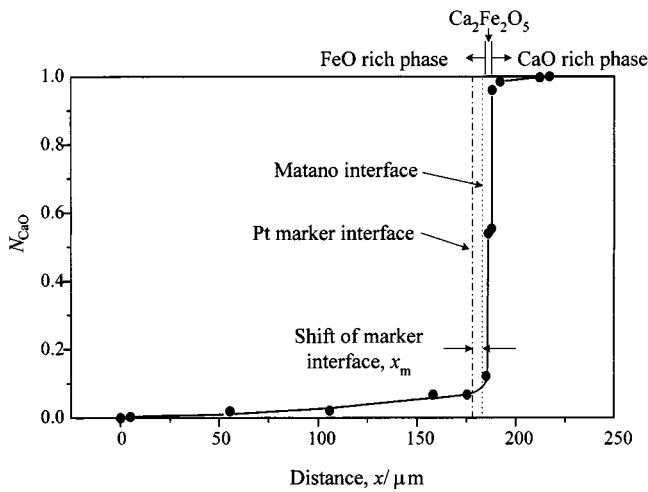


Fig. 6—Diffusion profile for the sample annealed with $P_{O_2} = 10^{-10}$ Pa at 1273 K for 0.6 ks.

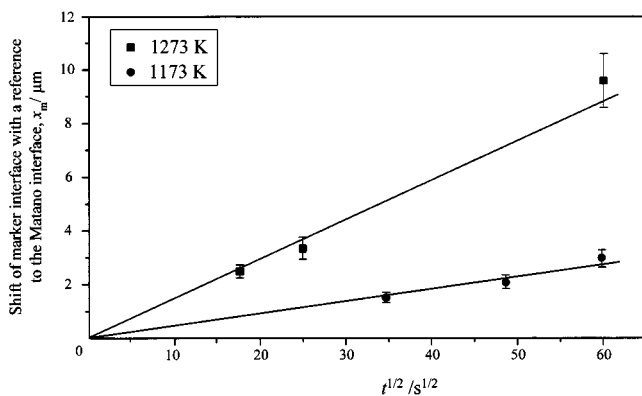


Fig. 7—Relation between the marker shift with a reference to the Matano interface and square root of the diffusion time at temperatures of 1173 and 1273 K.

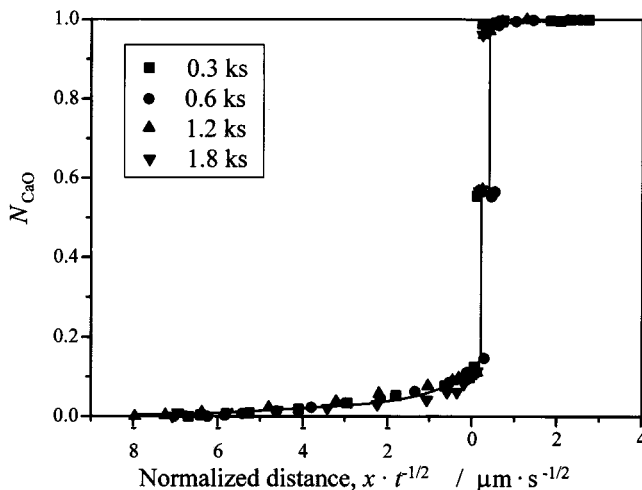


Fig. 8—Diffusion profile of CaO normalized by square root of diffusion time at 1273 K.

the pre-exponential factor, R is the gas constant (8.314 J/K·mol), and T is the absolute temperature. The values Q and D_0 are found to be independent of temperature within

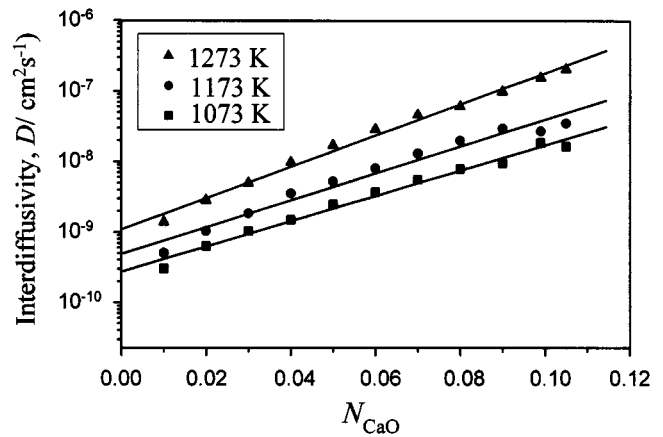


Fig. 9—Concentration dependence of interdiffusivity in the CaO-FeO system at temperatures of 1023, 1173, and 1273 K.

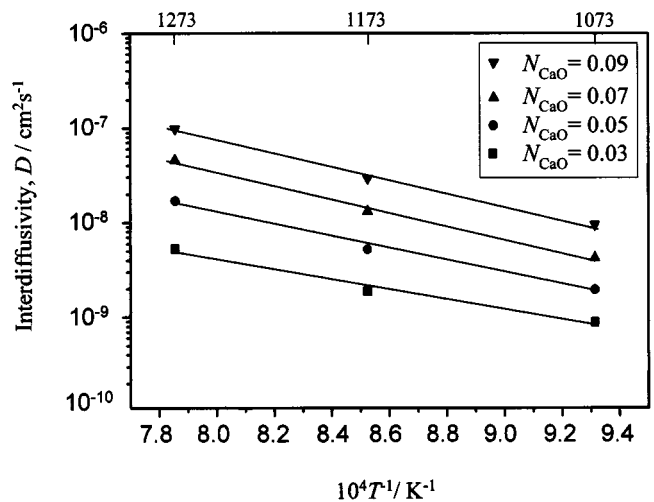


Fig. 10—Temperature dependence of interdiffusivity for several CaO contents in the FeO-CaO system.

Table II. Summary of Diffusion Results in the Form of Arrhenius-Type Formula, $D = D_0 \exp(-Q/RT)$, where $R = 8.314 \text{ J/mol} \cdot \text{K}$

| N_{CaO} | D_0 ($\text{cm}^2 \text{ s}^{-1}$) | Q (kJ mol^{-1}) |
|-----------|--|------------------------------|
| 0.09 | 1.3×10^{-1} | 145 |
| 0.07 | 5.1×10^{-2} | 142 |
| 0.05 | 8.2×10^{-3} | 129 |
| 0.03 | 2.3×10^{-4} | 97 |

the experimental accuracy. The equations for the straight lines plotted in the figure are listed in Table II. The activation energy increases with increasing CaO concentration.

E. Intrinsic Diffusivity

The intrinsic diffusivities, $D_{Ca^{2+}}$ and $D_{Fe^{2+}}$, have been determined from the velocity of the marker interface and the interdiffusivities. The intrinsic diffusivity values are presented at temperatures of 1273 and 1173 K in Table III. The intrinsic diffusivity of Fe^{2+} is slightly larger than that of Ca^{2+} at both temperatures.

Table III. Intrinsic Diffusivities of Ca²⁺ and Fe²⁺ in the FeO-CaO System at Temperatures of 1173 and 1273 K

| Temperature (K) | Concentration at Marker Position (N_{CaO}) | Interdiffusivity D ($\text{cm}^2 \text{s}^{-1}$) | Intrinsic Diffusivity of Fe ²⁺ $D_{\text{Fe}^{2+}}$ ($\text{cm}^2 \text{s}^{-1}$) | Intrinsic Diffusivity of Ca ²⁺ $D_{\text{Ca}^{2+}}$ ($\text{cm}^2 \text{s}^{-1}$) | Ca Impurity Diffusivity in FeO Single Crystal, $D_{\text{Ca}^{2+}}$ ($\text{cm}^2 \text{s}^{-1}$) ^[16] |
|-----------------|---|--|--|--|---|
| 1273 | 0.07 | 4.6×10^{-8} | 6.9×10^{-8} | 4.4×10^{-8} | 4.9×10^{-8} |
| 1173 | 0.08 | 2.0×10^{-8} | 2.1×10^{-8} | 1.7×10^{-8} | 1.3×10^{-8} |

Labidi *et al.*^[16] studied Ca impurity diffusion in single crystalline FeO under controlled oxygen-partial pressures at temperatures ranging from 1073 to 1423 K. The values extrapolated to the present experimental conditions using their regression formula are in excellent agreement with the present results, as shown in Table III.

IV. DISCUSSION

A. Solid-State Reaction Model

The vacancy mechanism can be accepted for diffusion in the present system. CaO and FeO are both rock-salt-type structure compounds where large anions are arranged in cubic close packing and all the octahedral interstitial sites are filled with cations. Schottky defects are thermally formed in both compounds, and the respective cations diffuse in counter ward each other through the cation vacancies with maintaining electrical neutrality at the diffusion interface. Thus, in general, the apparent activation energy, Q , determined consists of the heat of formation of cation vacancy and the activation energy of diffusion.

In the present system, some iron exists in a trivalent state, which makes the diffusion mechanism more complicated, because three Ca²⁺ could be replaced by two Fe³⁺ and a vacancy. Fe³⁺ becomes more stable with an increase in CaO content, which may lead to additional vacancy formation to the thermally created vacancies. Stabilization of Fe³⁺ by CaO eventually results in the formation of Ca₂Fe₂O₅. The solid-state reaction mechanisms relating to the formation of Ca₂Fe₂O₅ will be discussed based on the following characteristic results.

- (1) The Pt marker interface was always observed in the FeO phase relatively far from the Ca₂Fe₂O₅ layer, as shown in Figure 5. This would suggest that the Fe²⁺ diffuses much faster than Ca²⁺ across the diffusion interface.
- (2) However, the intrinsic diffusivity of Fe²⁺ is as large as that of Ca²⁺ at the marker position, as shown in Table III.
- (3) The Ca₂Fe₂O₅ phase grows according to the parabolic rate law, indicating that the process is diffusion-controlled.
- (4) The interface between the FeO solid solution and the Ca₂Fe₂O₅ presents the zigzag shape, as shown in Figures 3 and 5.

To explain the foregoing phenomena reasonably, the following reaction model is proposed and schematically illustrated in Figure 11.

- (a) The Ca₂Fe₂O₅ forms at the CaO-FeO interface at the beginning of the reaction as soon as the FeO/CaO couple is raised to the experimental temperature.
- (b) Assuming that $D_{\text{Fe}^{3+}} \gg D_{\text{Ca}^{2+}}$ in the Ca₂Fe₂O₅ phase, Fe³⁺ principally diffuses toward the CaO phase through

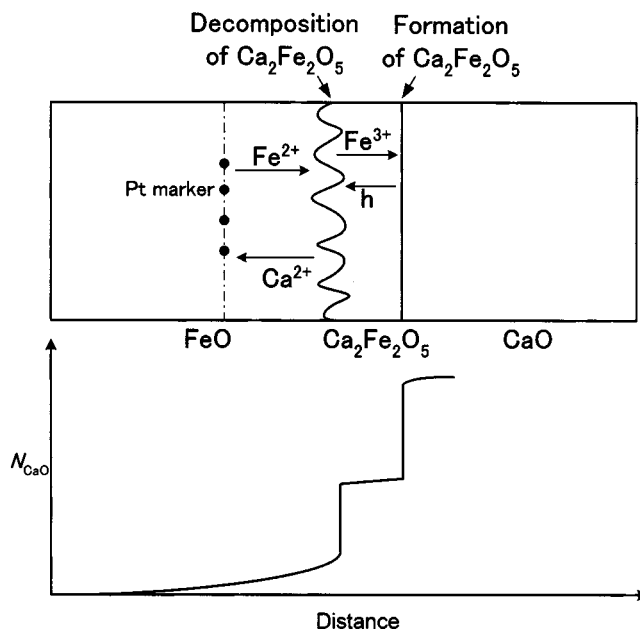
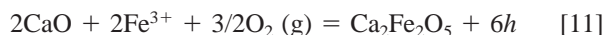


Fig. 11—Solid-state reaction model for the CaO and FeO system showing a cross-sectional view of a diffusion couple with diffusion profile.

the Ca₂Fe₂O₅ layer, while holes, h , diffuse in the counter direction to maintain electrical neutrality in the Ca₂Fe₂O₅.

- (c) The diffused Fe³⁺ reacts with CaO to form Ca₂Fe₂O₅ at the CaO-Ca₂Fe₂O₅ interface by the following reaction where CaO stabilizes Fe³⁺:



- (d) The Ca₂Fe₂O₅ decomposes simultaneously at the FeO-Ca₂Fe₂O₅ interface by the following reaction because of the dissolution of CaO into the FeO phase:



FeO reacts with the arriving holes at the interface, forming trivalent iron ions.



Thus, the resultant trivalent iron diffuses in the Ca₂Fe₂O₅ phase.

- (e) The decomposition of the Ca₂Fe₂O₅ may result in the zigzag shape of the interface between the FeO and Ca₂Fe₂O₅.
- (f) The growth rate of the Ca₂Fe₂O₅ phase depends on the diffusivities of Fe³⁺ in the Ca₂Fe₂O₅ phase and that of Ca²⁺ in the FeO phase. Therefore, the growth rate obeys the parabolic rate law, as shown in Figure 4.

It has been reported on the structure of Ca₂Fe₂O₅ that iron

Table IV. Evaluation of the Diffusivities of Fe³⁺ in the Ca₂Fe₂O₅ Phase at 1273 K with P_{O₂} = 10⁻¹⁰ Pa

| $dN_{\text{CaO}}/d \ln u$ at the FeO-C ₂ F Interface | D (cm ² s ⁻¹) at the FeO-C ₂ F Interface | Slope of the Line in Fig. 4 A (cm s ^{-1/2}) | At the CaO-C ₂ F Interface | At the FeO-C ₂ F Interface |
|---|--|--|---|---------------------------------------|
| | | | Activity of CaO, a_{CaO} | |
| | | | 0.97 | 0.21 |
| 3.27×10^{-1} | 2.0×10^{-7} | 4.41×10^{-6} | $D_{\text{Fe}^{3+}}/\text{cm}^2 \text{ s}^{-1}$ | |
| | | | 5.1×10^{-8} by Eq. [A11] | 3.5×10^{-8} by Eq. [A11] |
| | | | 5.7×10^{-8} by Eq. [A12] | 3.1×10^{-8} by Eq. [A12] |

C₂F = Ca₂Fe₂O₅.

in Ca₂Fe₂O₅ is both octahedrally and tetrahedrally coordinated by oxygen, while, calcium is coordinated by oxygen in a square antiprism.^[22] This indicates that the formation of the iron vacancy is much easier than that of calcium vacancy, supporting the present model. However, because the electrical conduction mechanism and cation diffusion data in Ca₂Fe₂O₅ are unknown, no further discussion on the reaction model can be made.

B. Diffusivity of Fe³⁺ in Ca₂Fe₂O₅

On a basis of the reaction model discussed in Section IV–A, the diffusivity of Fe³⁺ in Ca₂Fe₂O₅ is evaluated in the following manner. The growth rate of Ca₂Fe₂O₅ can be expressed by the difference between formation rate and dissolution rate.

$$\frac{dx}{dt} = j_{\text{Fe}^{3+}} \cdot V_m - j_{\text{Ca}^{2+}} \cdot V_m \quad [14]$$

where J_i is the flux of component, i , and V_m is the molar volume of CaFeO_{2.5}. The two terms on the right-hand side of Eq. [14] can be given by

$$j_{\text{Fe}^{3+}} \cdot V_m = \frac{V_m}{x} k_1 \quad [15]$$

$$j_{\text{Ca}^{2+}} \cdot V_m = \frac{V_m}{x} k_2 \quad [16]$$

where k_1 and k_2 are derived and given in the Appendix. Substituting Eqs. [15] and [16] into Eq. [14] and integrating from $t = 0, x = 0$ to $t = t, x = x$ gives

$$x^2 = 2(V_m k_1 - V_m k_2)t \quad [17]$$

Therefore, the term $2(V_m k_1 - V_m k_2)$ corresponds to the parabolic rate constant derived from Figure 4.

$$A^2 = 2(V_m k_1 - V_m k_2) \quad [18]$$

where A is the slope of the line shown in Figure 4. While, $V_m k_2$ also can be obtained from the penetration curve and the interdiffusivity as explained in the Appendix. Therefore, $V_m k_1$ can be calculated by Eq. [18], which enables us to estimate the value of $D_{\text{Fe}^{3+}}$ in the Ca₂Fe₂O₅ phase by using Eq. [A11] or [A12] in the Appendix. The Fe³⁺ vacancies are formed by the two possible dissolution reactions of CaO into Ca₂Fe₂O₅, as presented in the Appendix. Thus, the diffusivity of Fe₃₊ depends on the type of vacancy formation reaction, and the diffusivity of Fe³⁺ is a function of the activity of CaO. The results are tabulated in Table IV.

V. CONCLUSIONS

The solid-state reaction mechanisms of the CaO-FeO system have been studied by a diffusion couple method in the temperature range 1073 to 1273 K, under controlled oxygen-partial pressures. The Ca₂Fe₂O₅ formed at the interface and grew according to a diffusion-controlled process. The interdiffusivities and intrinsic diffusivities of Ca²⁺ and Fe²⁺ have been determined in the limited FeO solid-solution range. Based on the obtained results, a solid-state reaction model of the system has been proposed. The Ca₂Fe₂O₅ phase is formed at the CaO-Ca₂Fe₂O₅ interface and simultaneously decomposed at the FeO-Ca₂Fe₂O₅ interface because of the dissolution of CaO in the FeO phase. According to the model, the diffusivities of Fe³⁺ in the Ca₂Fe₂O₅ phase have been estimated at 1273 K.

APPENDIX

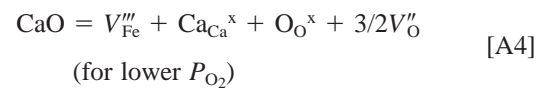
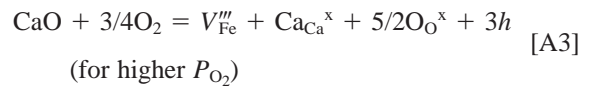
Regarding the growth rate of an intercompound formed by reactions at the interface of a diffusion couple, Wagner^[23,24] derived the relation between the rational reaction-rate constant, k , and the diffusivity of a rate-determining species. In the present study, Fe³⁺ is assumed to be the rate-determining species for the growth of Ca₂Fe₂O₅, and the rate constant, k_1 , can be expressed by

$$k_1 = -\frac{1}{RT} \int_{\mu_{\text{Fe}}(\text{FeO})}^{\mu_{\text{Fe}}(\text{CaO})} D_{\text{Fe}^{3+}} c_{\text{Fe}^{3+}} d\mu_{\text{Fe}} \quad [A1]$$

where $\mu_{\text{Fe}}(\text{CaO})$ and $\mu_{\text{Fe}}(\text{FeO})$ are the chemical potentials of Fe at the CaO-Ca₂Fe₂O₅ interface and the FeO-Ca₂Fe₂O₅ interface, respectively. $c_{\text{Fe}^{3+}}$ is the concentration of Fe³⁺ in mol/m³ in the Ca₂Fe₂O₅. The flux of Fe³⁺ is equal to that of Fe³⁺ vacancy:

$$D_{\text{Fe}^{3+}} c_{\text{Fe}^{3+}} = D_v [V_{\text{Fe}}'''] \quad [A2]$$

where D_v and $[V_{\text{Fe}}''']$ are the diffusivity and the concentration of Fe³⁺ vacancy, respectively. Assuming that $c_{\text{Fe}^{3+}}$ and D_v are constant under the present conditions, $D_{\text{Fe}^{3+}}$ is proportional to $[V_{\text{Fe}}''']$. Fe³⁺ vacancies are formed by the two possible dissolution reactions of CaO into Ca₂Fe₂O₅ in addition to the intrinsic defect formations, such as Schottky and Frenkel types of defects:



where Kröger–Vink notation is used. In the present study, we cannot determine which reaction is more favorable, because the oxygen partial-pressure dependence of the rate constant has not been determined. Therefore, $D_{\text{Fe}^{3+}}$ can be expressed in two ways by substituting the equilibrium relations of the preceding reactions and the electrical neutrality into Eq. [A2]:

$$D_{\text{Fe}^{3+}} = \frac{D_V}{c_{\text{Fe}^{3+}}} \left(\frac{K_{(A3)}}{3^3 [\text{Ca}_{\text{Ca}}^{\times}][\text{O}_{\text{O}}^{\times}]^{5/2}} \right)^{1/4} p_{\text{O}_2}^{3/16} a_{\text{CaO}}^{1/4} \quad [\text{A5}]$$

$$= D' p_{\text{O}_2}^{3/16} a_{\text{CaO}}^{1/4}$$

$$D_{\text{Fe}^{3+}} = \frac{D_V}{c_{\text{Fe}^{3+}}} \left(\frac{K_{(A4)}}{(3/2)^{3/2} [\text{Ca}_{\text{Ca}}^{\times}][\text{O}_{\text{O}}^{\times}]} \right)^{2/5} a_{\text{CaO}}^{2/5} = D'' a_{\text{CaO}}^{2/5} \quad [\text{A6}]$$

where $K_{(A3)}$ and $K_{(A4)}$ are the equilibrium constants of reactions [A3] and [A4], respectively. D' and D'' are as follows:

$$D' = \frac{D_V}{c_{\text{Fe}^{3+}}} \left(\frac{K_{(A3)}}{3^3 [\text{Ca}_{\text{Ca}}^{\times}][\text{O}_{\text{O}}^{\times}]^{5/2}} \right)^{1/4} \quad [\text{A7}]$$

$$D'' = \frac{D_V}{c_{\text{Fe}^{3+}}} \left(\frac{K_{(A4)}}{(3/2)^{3/2} [\text{Ca}_{\text{Ca}}^{\times}][\text{O}_{\text{O}}^{\times}]} \right)^{2/5} \quad [\text{A8}]$$

Taking account of the equilibrium relation:

$$\mu_{\text{Fe}} + 3/4 \mu_{\text{O}_2} + \mu_{\text{CaO}} = \mu_{\text{CaFeO}_{2.5}} \quad [\text{A9}]$$

the following equation can be obtained for the fixed chemical potential of oxygen in $\text{CaFeO}_{2.5}$:

$$d\mu_{\text{Fe}} = -d\mu_{\text{CaO}} = -RT d \ln a_{\text{CaO}} \quad [\text{A10}]$$

Substituting Eqs. [A7], [A8], and [A10] into Eq. [A1] gives:

$$V_m k_1 = D' p_{\text{O}_2}^{3/16} \int_{\ln a_{\text{CaO}}(\text{FeO})}^{\ln a_{\text{CaO}}(\text{CaO})} a_{\text{CaO}}^{1/4} d \ln a_{\text{CaO}} \quad [\text{A11}]$$

$$= 4D' p_{\text{O}_2}^{3/16} [a_{\text{CaO}}]_{a_{\text{CaO}}(\text{FeO})}^{a_{\text{CaO}}(\text{CaO})}$$

$$V_m k_1 = D'' \int_{\ln a_{\text{CaO}}(\text{FeO})}^{\ln a_{\text{CaO}}(\text{CaO})} a_{\text{CaO}}^{2/5} d \ln a_{\text{CaO}} \quad [\text{A12}]$$

$$= \frac{5}{2} D'' [a_{\text{CaO}}]_{a_{\text{CaO}}(\text{FeO})}^{a_{\text{CaO}}(\text{CaO})}$$

where $V_m = 1/c_{\text{Fe}^{3+}}$. Takeda and Yazawa^[25,26] reported the activity data in the CaO-FeO system at 1473 to 1573 K. According to their results, the activities of CaO present slightly positive deviation from an ideal solution in the FeO solid solution. It is, therefore, reasonable to obtain the activity value of CaO at 1273 K by the regular solution model based on their results in the FeO solid solution. Since the solid solubility is very limited in the CaO solid solution, the ideal solution model can be applied without causing large errors. The estimated CaO activities in both solid solutions at 1273 K were presented in Table IV.

On the other hand, k_2 can be related to $j_{\text{Ca}^{2+}}$ by using Fick's first law in the FeO solid-solution range as:

$$k_2 \equiv j_{\text{Ca}^{2+}} \cdot x = - \left(D \frac{dc_{\text{Ca}^{2+}}}{dx} \right) x \quad [\text{A13}]$$

where $c_{\text{Ca}^{2+}}$ is only a function of $u (=x/t^{1/2})$, as shown in Figure 8. The molar fraction of CaO , N_{CaO} , is given by

$$N_{\text{CaO}} = \frac{c_{\text{Ca}^{2+}}}{c} \quad [\text{A14}]$$

where c is the total number of moles per unit volume. Substituting Eq. [A14] and the function u into Eq. [A13] gives

$$V_m k_2 = -D \frac{dN_{\text{CaO}}}{d \ln u} \quad [\text{A15}]$$

where cV_m is assumed as unity.

REFERENCES

1. *Volume Reduction and Recycling of Steel Slag*, Iron and Steel Institute of Japan, Tokyo, 1997, pp. 157-212 (in Japanese).
2. R. Inoue and H. Suito: *Iron Steel Inst. Jpn. Int.*, 1995, vol. 35 (3), pp. 272-79.
3. W.C. Allen and R.B. Snow: *J. Am. Ceram. Soc.*, 1955, vol. 38 (8), pp. 264-80.
4. B. Phillips and A. Muan: *Trans TMS-AIME*, 1960, vol. 218, pp. 1112-18.
5. F. Abbtista, A. Burdese, and M. Maja: *Rev. Int. Hautes Temp. Refract.*, 1975, vol. 12 (4), pp. 337-42; cited in Ref. 8.
6. R.E. Johnson and A. Muan: *J. Am. Ceram. Soc.*, 1965, vol. 48 (7), p. 360.
7. E. Schürmann and G. Kraume: *Arch. Eisenhüttenwes.*, 1976, vol. 47 (6), pp. 327-31.
8. B. Bergman and C. Song: *J. Am. Ceram. Soc.*, 1988, vol. 71 (3), pp. C-121-C-125.
9. M. Hillert, M. Selleby, and B. Sundman: *Metall. Trans. A*, 1990, vol. 21A, pp. 2759-75.
10. R.W. Gurry and L.S. Darken: *Am. Chem. Soc. J.*, 1950, vol. 72, pp. 3906-10.
11. B. Björkman: *Scand. J. Metall.*, 1984, vol. 13, pp. 193-200.
12. B. Bergman: *J. Am. Ceram. Soc.*, 1986, vol. 69 (8), pp. 608-11.
13. A. van Sandwijk and K. Koopmans: in *Science of Ceramics*, H. Hausner, ed., Deutsche Keramische Gesellschaft, Bad Honnef, Germany, 1980, vol. 10, pp. 403-09.
14. R.E. Carter and F.D. Richardson: *Trans. AIME, J. Met.*, 1954, pp. 1244-57.
15. L. Himmel, R.F. Mehl, and C.E. Birchenall: *Trans. AIME, J. Met.*, 1953, pp. 827-43.
16. M. Labidi, H. Boussetta, and C.J.A. Monty: *Solid State Ionics*, 1997, vol. 104, pp. 133-45.
17. B. Philips and A. Muan: *J. Phys. Chem.*, 1960, vol. 64 (10), pp. 1451-53.
18. P. Shewmon: *Diffusion in Solids*, 2nd ed., TMS, Warrendale, PA, 1989, pp. 34-37.
19. W. Jost: *Z. Phys.*, 1950, vol. 127, pp. 163-67.
20. M. Appel: *Scripta Metall.*, 1968, vol. 2, pp. 217-22.
21. L.S. Darken: *Trans. AIME, J. Met.*, 1948, vol. 174, pp. 184-94.
22. J. Berggren: *Acta Chem. Scand.*, 1971, vol. 25 (10), pp. 3616-24.
23. C. Wagner: *Z. Phys. Chem.*, 1936, vol. 34, pp. 309-16.
24. K. Kawamura, A. Saiki, T. Maruyama, and K. Nagata: *J. Electrochem. Soc.*, 1995, vol. 142 (9), pp. 3073-77.
25. Y. Takeda and A. Yazawa: *Nippon Kogyokaiishi*, 1980, vol. 96, pp. 901-06.
26. *Slag Atlas*, 2nd ed, Verein Deutscher Eisenhüttenleute (VDDeh), Verlag Stahleisen GmbH, D-Düsseldorf, 1995, p. 229.